Article ID: 1006-8775(2024)02-0097-09

Linkage Between European and East Asian Heatwaves on Synoptic Scales

CAI Fen-ying (蔡奋颖)[1,2], LIU Cai-hong (刘彩红)[3], YANG Song (杨 崧)[1,4], DENG Kai-qiang (邓开强)[1], KURTHS Jürgen[2,5]

(1. School of Atmospheric Sciences, Sun Yat-sen University, and Southern Marine Science and Engineering Guangdong Laboratory (Zhuhai), Zhuhai, Guangdong 519082 China; 2. Department of Complexity Science, Potsdam Institute for Climate Impact Research (PIK), Member of the Leibniz Association, Potsdam 14473 Germany; 3. Department of Water and Climate Risk, Institute for Environmental Studies, Vrije Universiteit Amsterdam, Amsterdam 1087HV Netherlands; 4. Guangdong Province Key Laboratory for Climate Change and Natural Disaster Studies, Sun Yat-sen University, Zhuhai, Guangdong 519082 China; 5. Department of Physics, Humboldt-Universität zu Berlin, Berlin 12489 Germany)

Abstract: Concurrent extreme weather events in geographically distant areas potentially cause high-end risks for societies. By using network analysis, the present study managed to identify significant nearly-simultaneous occurrences of heatwaves between the grid cells in East Asia and Eastern Europe, even though they are geographically far away from each other. By further composite analysis, this study revealed that hot events first occurred in Eastern Europe, typically with a time lag of 3–4 days before the East Asian heatwave events. An eastward propagating atmospheric wave train, known as the circum-global teleconnection (CGT) pattern, bridged the sequent occurrences of extreme events in these two remote regions. Atmospheric blockings, amplified by surface warming over Eastern Europe, not only enhanced local heat extremes but also excited a CGT-like pattern characterized by alternative anomalies of high and low pressures. Subsequent downstream anticyclones in the middle and upper troposphere reduced local cloud cover and increased downward solar radiation, thereby facilitating the formation of heatwaves over East Asia. Nearly half of East Asian heatwave events were preceded by Eastern European heatwave events in the 10-day time range before East Asian heatwave events. This investigation of heatwave teleconnection in the two distant regions exhibits strong potential to improve the prediction accuracy of East Asian heatwaves.

Key words: concurrent heatwaves; Eastern Europe; East Asia; circum-global teleconnection pattern

CLC number: P466 **Document code:** A

Citation: CAI Fen-ying, LIU Cai-hong, YANG Song, et al. Linkage Between European and East Asian Heatwaves on Synoptic Scales [J]. Journal of Tropical Meteorology, 2024, 30(2): 97–105, https://doi.org/10.3724/j.1006-8775.2024.010

1 INTRODUCTION

Heatwaves, identified as an extended period of anomalously high temperatures (Fischer and Schär [1]; Perkins and Alexander [2]), potentially exert overwhelming impacts on human societies and ecosystems (Westerling et al. [3]; Thornton et al. [4]; Meng et al. [5]; Rübbelke and Vögele [6]; Coumou and Rahmstorf [7]; Lesk et al. [8]). For example, the devastating hot summer of 2003 caused around 40,000 heat-related deaths and sizable agricultural production losses across Europe (Fouillet et al. [9]; García-Herrera et al. [10]; Laaidi et al. [11]). This was not occasional, and European extreme hot events recurred in 2010 (Barriopedro et al. [12]; Dole et al. [13]), 2015 (Russo et al. [14]; Duchez et al. [15]), and 2022 (Wang et al. [16]). Another example in Southwest China in 2022 featured extreme heatwaves associated with droughts and wildfires, brought about rippling socioeconomic and environmental impacts, including drinking water shortage, agricultural loss, electricity crunch and human health risk (Chen et al. [17]). On a global scale, heat extremes draw world-wide concerns, since both their intensity and frequency show increasing trends in the recent warming decades (Perkins et al. [18]; Coumou and Rahmstorf [7]; Mazdiyasni and AghaKouchak [19]; Perkins and Lewis [20]; Rousi et al. [21]) and are expected to increase continuously in the future roasting climate (Meehl and Tebaldi [22]; Coumou and Robinson [23]; Christidis et al. [24]; King and Harrington [25]; Zhang et al. [26]).

Compared with a single extreme weather event, compound or multiple events have recently sparked stronger scientific interests because amplified societal impacts are often observed for such concurrent extremes (Zscheischler and Seneviratne [27]; Sarhadi et al. [28]). Several studies have revealed that recurring concurrences of climate extremes are not in coincidence, including extreme rainfall synchronization (Boers et al. [29–31]; Gupta et al. [32]; Su et al. [33]), heatwave-flood teleconnection

Received 2023-11-23; **Revised** 2024-02-15; **Accepted** 2024-6-7

Funding: Guangdong Major Project of Basic and Applied Basic Research (2020B0301030004); National Natural Science Foundation of China (42275020); Innovation Group Project of Southern Marine Science and Engineering Guangdong Laboratory (Zhuhai) (311021001); Guangdong Province Key Laboratory for Climate Change and Natural Disaster Studies (2020B1212060025)

Biography: CAI Fen-ying, primarily undertaking research on global teleconnections of weather extremes based on network analysis.

Corresponding author: YANG Song, e-mail: yangsong3@mail.sysu.edu.cn

(Lau and Kim [34]; Capua et al. [35]), compound drought and heatwave events (Mazdiyasni and AghaKouchak [19]; Li et al. [36]; Mukherjee and Mishra [37]), and concurrent heat extremes along the mid-latitude westerly jet streams in the Northern Hemisphere (Kornhuber et al. [38, 39]). Kornhuber et al. [39] indicated that heat extremes over Eastern Europe and East Asia occurred nearly simultaneously and were associated with the recurrent Rossby wave pattern with wave number 5. A congruous result was concluded by Yang et al. [40], despite the fact that lead-lag information on the occurrences of distant heatwaves was not discussed thoroughly in these studies. In addition, the days of European and East Asian summer heatwaves vary consistently on interannual time scales, for which the sea surface temperature anomaly in the Atlantic Ocean is a common driver (Zhou and Wu [41]; Deng et al. [42]).

However, the lead-lag relationship between the occurrences of European and East Asian heatwaves on synoptic time scales is still unclear. Which happens first compared with the other? What is the time lag between their occurrences? How are they bridged between the two distant regions? This study aims to clarify the lead-lag concurrences of heat extremes over Eurasia and the responsible physical mechanisms for heatwave teleconnection. Section 2 describes the datasets and methods used in this study. The results obtained are illustrated in section 3, followed by a summary and discussion in section 4.

2 DATA AND METHODS

We adopt the ERA5 reanalysis dataset (Hersbach et al. [43]) in this study. Hourly data on surface and ten pressure levels (1000, 925, 850, 700, 600, 500, 400, 300, 200, 100 hPa), with a horizontal resolution of 1.0°×1.0°, are averaged into daily means preparatory for further composite analysis. There are a total of 3956 days in our analysis period, June–July–August (JJA) of 1979–2021. Physical variables, including 2-m temperature (T2m), total cloud cover (TCC), solar radiation, multilevel atmospheric temperature, geopotential height, zonal wind and meridional wind, are analyzed in this study.

Heatwave day on a 1.0°×1.0° grid cell in land areas is identified when daily T2m exceeds its 90th percentile threshold for at least three consecutive days, as in previous studies (Fischer and Schär [1]; Perkins and Alexander [2]). The 90th percentile threshold on each date is calculated from a total of 43 years × 15 days (7 days on either side of the target day). For instance, the threshold value on June 15 equals the 90th percentile of T2m from June 8 to June 22 during 1979–2021 (645 days).

To explore the concurrences of heatwaves over different regions, we apply a network analysis in this study. The strength of a link between grid cells a and b is defined as the concurrent days, when heatwaves occur simultaneously over grid cells a and b. We shuffle the daily heatwaves (absence as 0 or presence as 1) time series 1000 times for each grid cell, and then calculate the 99th threshold of link strengths for each pair of grid cells (a, b) from the shuffled data. When the real strength of a link is lower than the 99th threshold, this link is identified as nonsignificant and will be removed. Furthermore, the degree strength is identified as the weighted sum of the link strengths, and each link is weighted by $\cos\left((\text{latitude}_a + \text{latitude}_b)/2\right)$. In particular, the degree strength of a grid cell inside East Asia (D^{EA}) is the weighted sum of the links between this grid cell and grid cells in East Asia (Fig. 1a). Similarly, the degree strength D^{EE} is the weighted sum of link strengths inside Eastern Europe (Fig. 1b).

Regional heatwave days are identified when the number of heatwave grid cells in this region is higher than a certain value. In particular, about 10% (401 days) of the 3956 summer days are recognized as East Asian heatwave events when heatwaves occur in no less than 80 grid cells over 20°–45°N, 100°–125°E. The first day of each East Asian heatwave event is denoted as A0. The days after A0 are symbolized as A1 (i.e., A0 + 1 day), A2, A3, …, while the days before A0 are signified as B1 (i.e., A0 –1 day), B2, B3, …, etc. Similarly, Eastern European heatwave events are identified when heatwaves occur in no less than 130 grid cells over 50°–70°N, 15°–50°E, so that about 10% (398 days) of the summer days are selected as the Eastern European heatwave days.

To further investigate the development of East Asian surface warming and related physical processes, we conduct a composite analysis. There are three categories: A0–A1, B1–B2, and B3–B4. Category A0–A1 includes days A0 and A1, but those days A1 without the occurrences of East Asian heatwave events are excluded. Moreover, categories B1–B2 and B3–B4 include days that are two days and four days before the days in category A0–A1, respectively. Furthermore, days of June 1 to June 4 in categories A0–A1 are excluded so that days in categories B1–B2 and B3–B4 are still within the range

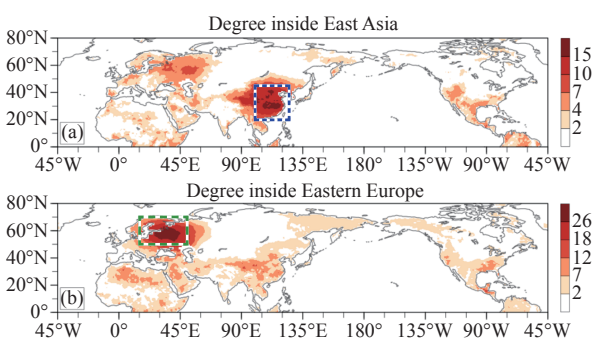

Figure 1. Degree strengths (units: 10^3) inside (a) East Asia (D^{EA}), and (b) Eastern Europe (D^{EE}). D^{EA} (D^{EE}) over a grid cell is the summed strengths of all significant links between this grid cell and the grid cells in East Asia (Eastern Europe). The strength of a link between grid cells a and b is identified by counting the concurrent days without delay when heatwaves occur over both grid cells a and b. The domains of East Asia (20°–45°N, 100°–125°E) and Eastern Europe (50°–70°N, 15°–50°E) are denoted by the blue box in (a) and green box in (b), respectively.

from June to August. There are 155 days in each category. Composite anomalies are the differences between the average physical variables in each category (155 days) and the climatology (3956 days). Student's *t*-test is used to test whether composite anomalies are significant, which are provided by the NCL function "ttest" (https://www.ncl.ucar.edu/Document/Functions/Built-in/ttest.shtml).

To investigate the wave packets related to Eurasian heatwaves, an empirical orthogonal function (EOF) analysis is performed for the yearly anomalies of meridional wind at 200 hPa (V200) during JJA of 1979–2021. Following previous studies (Yasui and Watanabe [44]; Cen et al. [45]), a circum-global teleconnection (CGT) pattern is identified as the first leading mode of V200 over 20°–60°N, 0°–150°E (Fig. 2a), since its major characteristic is observed near the Asian jet stream. The EOF approach is provided by the NCL function "eofunc" (https://www.ncl.ucar.edu/Document/Functions/Built-in/eofunc.shtml).

Furthermore, the propagation of atmospheric Rossby waves can be described by the wave activity flux (Takaya and Nakamura [46]), which can be written as follows:

$$W=\frac{p\cos\varphi}{2\left|\overline{U}\right|}\begin{bmatrix}\dfrac{\overline{u}}{a^2\cos^2\varphi}\left(\left(\dfrac{\partial\psi'}{\partial\lambda}\right)^2-\psi'\dfrac{\partial^2\psi'}{\partial\lambda^2}\right)+\dfrac{\overline{v}}{a^2\cos\varphi}\left(\dfrac{\partial\psi'}{\partial\lambda}\dfrac{\partial\psi'}{\partial\varphi}-\psi'\dfrac{\partial^2\psi'}{\partial\lambda\,\partial\varphi}\right)\\ \dfrac{\overline{u}}{a^2\cos\varphi}\left(\dfrac{\partial\psi'}{\partial\lambda}\dfrac{\partial\psi'}{\partial\varphi}-\psi'\dfrac{\partial^2\psi'}{\partial\lambda\,\partial\varphi}\right)+\dfrac{\overline{v}}{a^2}\left(\left(\dfrac{\partial\psi'}{\partial\varphi}\right)^2-\psi'\dfrac{\partial^2\psi'}{\partial\lambda^2}\right)\end{bmatrix}$$

where p = pressure (per 1000 hPa), while φ, λ, and a are latitude, longitude, and earth radius, respectively. Moreover, ψ' represents the anomaly of the stream function, while $\overline{U}$, $\overline{u}$, and $\overline{v}$ indicate the climatology of the wind speed, zonal wind, and meridional wind, respectively.

3 CONCURRENT HEATWAVES OVER EASTERN EUROPE AND EAST ASIA

Figure 1 shows the degree strengths inside East Asia (D^{EA}) and Eastern Europe (D^{EE}). High degree strengths indicate high simultaneous occurrences of heatwave days with East Asian heatwaves or Eastern European heatwaves. In addition to local synchronisation, East Asian heatwaves usually occur simultaneously with the heat extremes over Eastern Europe, the Middle East, and Southern North America (Fig. 1a). It is noticeable that the highest degree strengths D^{EA} are over Eastern Europe. Therefore, degree strengths inside Eastern Europe heatwaves (D^{EE}) are investigated further. Consistently, East Asian heatwaves are found to be highly synchronized with Eastern European heatwaves (Fig. 1b). Meanwhile, the heat extremes over the Middle East, Northeast Asia, and Southern North America are also correlated to the Eastern European heatwaves (Fig. 1b), implying strong links of heatwaves among these regions. However, investigating the details of extreme event teleconnection around the globe is beyond the scope of this article. In the following, we will focus on the remarkable simultaneous occurrences of heatwaves over Eastern Europe and East Asia.

To further analyze the lead-lag details of the nearly-simultaneous remote heatwaves over Eurasia, we conduct a composite analysis for East Asian heatwave events. The differences in T2m and atmospheric circulations between the climatology and the days in the categories A0–A1, B1–B2, and B3–B4 for East Asian heatwaves are shown in Fig. 3. For East Asia, T2m experiences a rapid increase before the onset of East Asian heatwaves (Figs. 3a, 3c, and 3e). The sudden surface warming over East Asia could be attributed to the formation of anticyclonic circulation anomalies in the middle- and upper-troposphere over East Asia (Figs. 3b, 3d, and 3f; Figs. 6b, 6e, and 6h). On the one hand, the anticyclone-related subsidence causes adiabatic heating in the entire troposphere (Figs. 4d and 4f). On the other hand, the reduction of total cloud cover and the increase in downward solar radiation also favor abrupt atmospheric heating near the surface (Figs. 3b, 3d, and 3f). For Eastern Europe, similar processes are involved, including anticyclonic circulation anomalies, enhanced adiabatic heating, less cloud cover, and more downward solar radiation (Fig. 3; Figs. 4a, and 4c).

It should be noted that the near-surface warming over Eastern Europe occurs about 2–4 days ahead of that over East Asia (Figs. 3a, 3c, and 3e). To exhibit the lead-lag

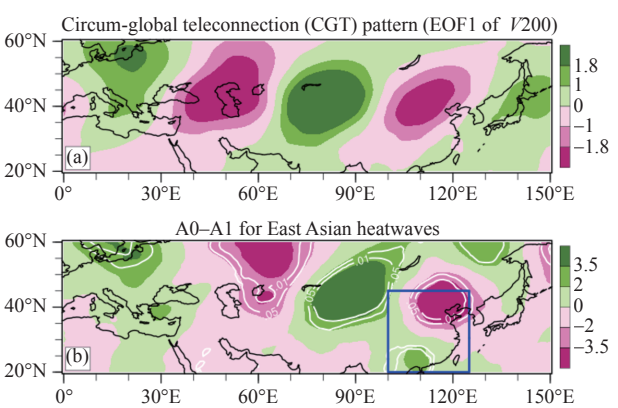

Figure 2. (a) Circum-global teleconnection pattern represented by the leading EOF mode of meridional wind at 200 hPa (V200) over 20°–60°N, 0°–150°E. The EOF result is calculated from the JJA mean (yearly) fields from 1979 to 2021, which are obtained from the ERA5 dataset. (b) Composite anomalies of V200 (shadings; units: m s^{-1}) for the category A0–A1 of East Asian heatwave events from the climatology. The contours in (b) denotes the statistically significant composite differences (p = 0.05 and p = 0.01). The blue box in (b) indicates the area of East Asia (20°–45°N, 100°–125°E). The pattern correlation between (a) and (b) is 0.61, significant at the 99.9% confidence level.

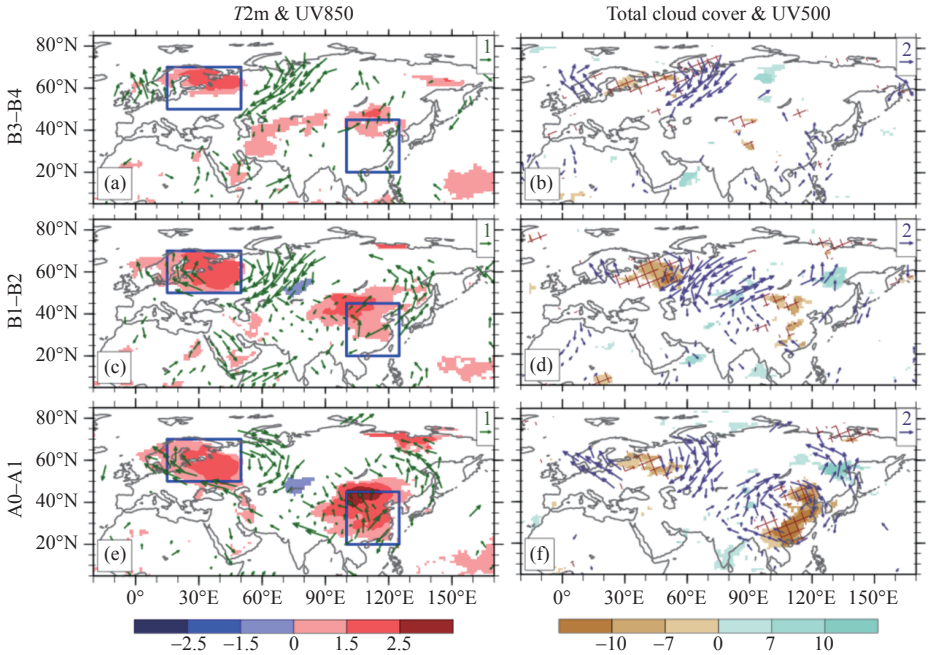

Figure 3. Composite anomalies of (a, c, e) air temperature at 2 m (shadings; units: K), and (b, d, f) total cloud cover (shadings; units: %). The anomalies of atmospheric circulation (colored vectors; units: m s^{-1}) at 850 hPa and 500 hPa are also shown in (a, c, e) and (b, d, f), respectively. Composite anomalies are the averaged differences between the climatology and days in a certain category. (e, f) are the differences between climatology and the category A0–A1 of East Asian heatwaves, while (c, d) and (a, b) are for category B1–B2 and B3–B4, respectively. Only the statistically significant values at the 95% confidence level are plotted. The red stippling in (b, d, f) denotes significant positive deviations of downward solar radiation from climatology (p<0.05). The blue boxes in (a, c, e) denote the areas of Eastern Europe (50°–70°N, 15°–50°E) and East Asia (20°–45°N, 100°–125°E).

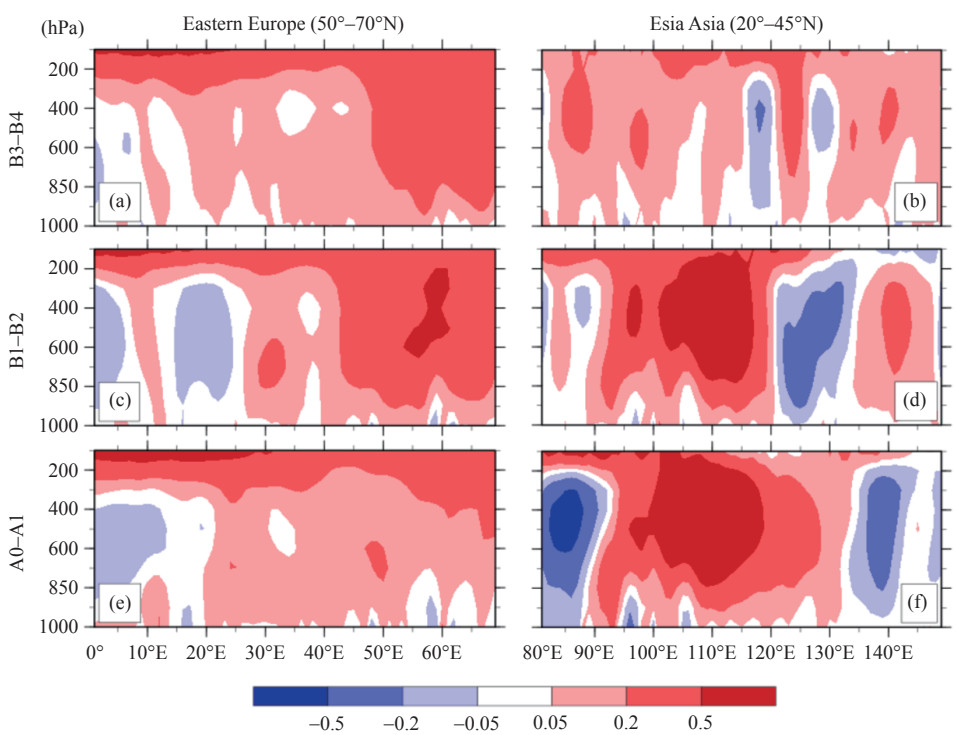

Figure 4. Composite anomalies of adiabatic heating ($-\left(\frac{p}{p_0}\right)^{\frac{R}{C_p}} \cdot \omega \cdot \frac{\partial \theta}{\partial p}$; units: K day^{-1}) averaged over (a, c, e) 50°–70°N, and (b, d, f) 20°–45°N. (e, f) are the composite anomalies for the category A0–A1 of East Asian heatwaves from the climatology, while (c, d) and (a, b) are for the categories B1–B2 and B3–B4, respectively.

coexistences of heatwaves over the two distant regions clearly, the composite anomalies of both *T*2m and geopotential height at 500 hPa (*H*500) are plotted in Fig. 5 for the Eastern European and East Asian heatwaves. *H*500 is analyzed here because surface heatwaves are often related to the middle tropospheric high-pressure center (Deng et al. [47, 48]). This way, we find that after a short period of rapid intensification, the surface warm center and middle-tropospheric high-pressure center usually reach their peaks on the second day (A1) of regional heatwave events (Fig. 5). In all four composite plots of *T*2m and *H*500, the East Asian and Eastern European peaks (i.e., highest composite anomalies) are significantly deviated from the climatology. Obviously, East Asian peaks are preceded by the Eastern European peaks, with a time lag of 3–4 days, indicating evident nearly simultaneous happenings between heat extremes over these two regions. In particular, on the sixth day (B6) before the occurrences of East Asian heatwaves, no significant East Asian *T*2m and *H*500 are observed (Figs. 5a and 5b). By contrast, significant positive anomalies of Eastern European *T*2m and *H*500 from the climatology (p<0.01) are observed (Figs. 5a and 5b) on the B6 before East Asian heatwaves. In the following several days, sudden atmospheric warming occurred over East Asia accompanying with the occurrences of East Asian heatwaves (Fig. 5a). In summary, notable significant positive anomalies of Eastern European *T*2m and *H*500 from the climatology (p<0.01) are observed in nearly a week ahead of the sudden atmospheric warming over East Asia (Figs. 5a and 5b), which is potentially helpful for predicting the occurrences of East Asian heatwaves.

4 PHYSICAL MECHANISM FOR THE TELECONNECTION OF HEAT EXTREME

Extreme weather events over distant regions could be connected by upper-tropospheric Rossby waves (Boers et al. [31]; Kornhuber et al. [39]). To clarify the physical causes associated with the lead-lag linkage between European and East Asian heatwaves on synoptic scales, we analyze the composite fields of atmospheric circulation, stream function, and wave flux activity at 300 hPa (Figs. 6a, 6b, 6d, 6e, 6g, and 6h). An eastward-propagating wave train, with alternative anticyclonic and cyclonic circulation anomalies, is observed over the Eurasian continent (Figs. 6a, 6d, and 6g). An anomalous upper-tropospheric anticyclone first appears over Eastern Europe, corresponding to the appearance of Eastern European heatwaves (Fig. 6b). Subsequently, an anomalous cyclone emerges over central Russia (Fig. 6e), accompanied with near-surface cooling (Figs. 3c and 3e). Four days later, another anomalous anticyclone appears over East Asia when heatwaves happen over the southeastern part of the Eurasian continent (Fig. 6h).

Such an eastward-propagating anticyclone-cyclone-anticyclone circulation pattern seems to be triggered by heatwave-related tropospheric warming over Eastern Europe (Fig. 6). Cen et al. [45] indicated that the tropospheric atmospheric heating over Eastern Europe could enhance an eastward propagating wave train resembling the CGT pattern. Formulated on an EOF analysis of yearly summertime *V*200 according to a previous study (Yasui and Watanabe [44]), the CGT pattern is identified as four alternative anomalies of upper-tropospheric northerlies and southerlies over Eurasia (Fig. 2a), which is mostly similar to the regression pattern of *V*200 onto another CGT index (Fig.

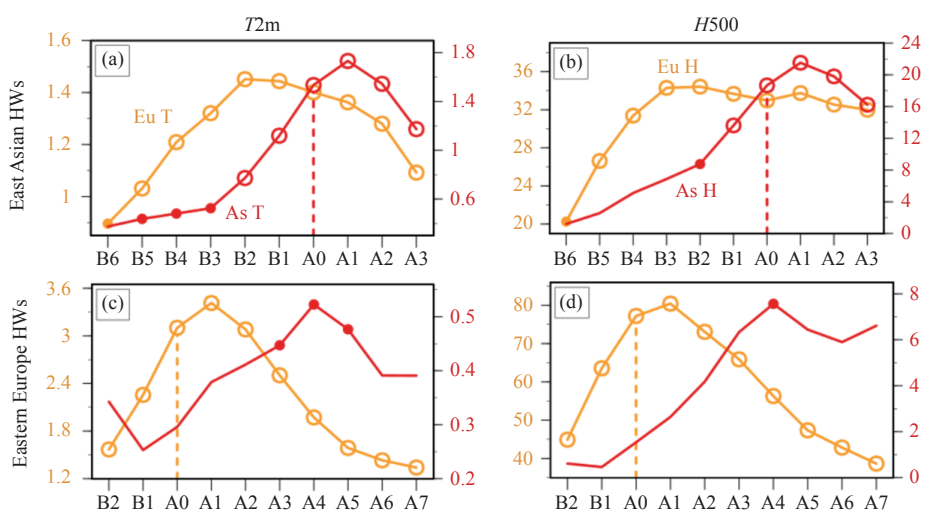

Figure 5. Composite anomalies of (a, c) atmospheric temperature at 2 m (units: K) and (b, d) geopotential height at 500 hPa (units: gpm). The composite fields are differences between the climatology and the regional heatwave days for (a, b) from 6 days before (B6) to 3 days after (A3) the East Asian heatwave events, and (c, d) from 2 days before (B2) to 7 days after (A7) the Eastern European heatwave events. Orange-yellow lines indicate the areal-averaged values over Eastern Europe (left dashed axes; 50°–70°N, 15°–50°E), while the red lines are for East Asia (right dashed axes; 20°–45°N, 100°–125°E). The composite anomalies are the differences between the averaged *T*2m or *H*500 in days A0 (or other days) and the climatology. The hollow circles (solid dots) are plotted when the differences are significant at the 99% (95%) confidence level.

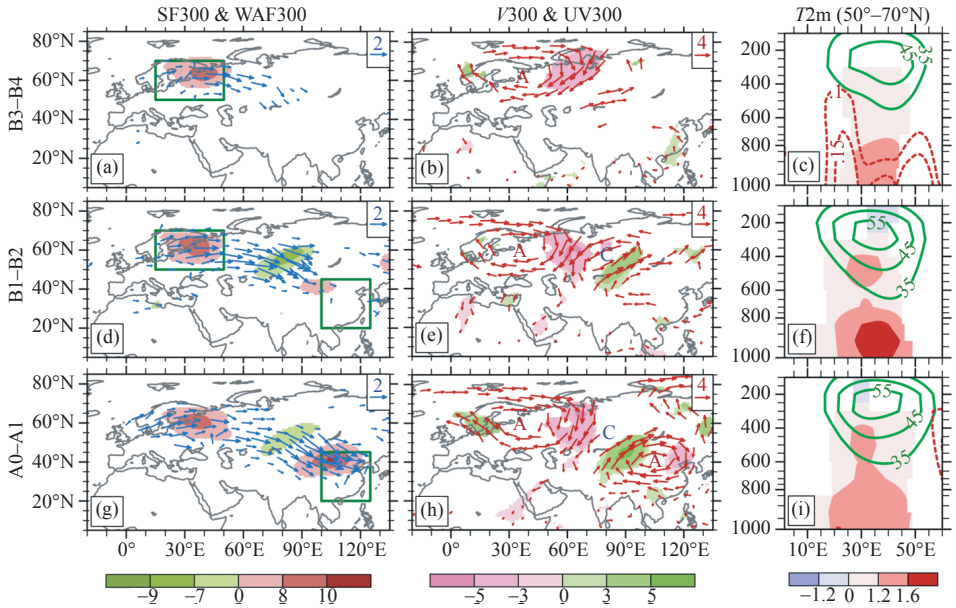

Figure 6. Composite anomalies of (a, d, g) stream function (shadings; units: 10^6 m^2 s^{-1}) and wave activity flux (vectors; units: m^2 s^{-2}) at 300 hPa, and (b, e, h) meridional wind (shadings; units: m s^{-1}) and atmospheric circulation (vectors; units: m s^{-1}) at 300 hPa. (c, f, i) are meridional averaged anomalies over 50°–70°N for atmospheric temperature (shadings; units: K), geopotential height (green solid contours; units: gpm), and atmospheric temperature tendency (red dashed contours; units: K day^{-1}). The plotted deviations of stream functions, meridional wind, wind vectors, and atmospheric temperature are all statistically significant at the 95% confidence level. Wave activity fluxes are not shown when both directions are less than 0.5 m^2 s^{-2} or both stream function anomalies and wind anomalies are insignificant. (g, h, i) are composite fields for the category A0–A1 of East Asian heatwaves, while (d, e, f) and (a, b, c) are for the categories B1–B2 and B3–B4, respectively. The green boxes in (a, d, g) denote the area of Eastern Europe (50°–70°N, 15°–50°E) and East Asia (20°–45°N, 100°–125°E).

2a in Zhou et al. [49]; Ding and Wang [50]). Reasonably, the heatwave-related wave train in this study seems to be a part of the CGT-like pattern (Lu et al. [51]; Ding and Wang [50]; Yasui and Watanabe [44]; Wang et al. [52]), as the pattern correlation coefficient between the composite *V*200 anomalies for category A0–A1 of Asian heatwaves and CGT-related *V*200 is up to 0.61 (Figs. 2a and 2b), which is significant at the 99.9% confidence level.

In particular, the upper-tropospheric high-pressure center and anticyclonic circulation anomalies are amplified by the sudden near-surface atmospheric warming over Eastern Europe, corresponding to the appearance of Eastern European heatwaves (Figs. 6a, 6c, 6d, and 6f). In the subsequent days, wave energy propagates toward the downstream regions and another anomalous anticyclone is excited over East Asia to stimulate the incidence of East Asian heatwaves (Fig. 3e; Figs. 6g and 6h).

5 SUMMARY AND DISCUSSION

This study investigates the lead-lag occurrences of European and East Asian heatwaves on synoptic timescale. Based on network analysis and composite analysis, a significant event synchronization with a time delay of 3–4 days is uncovered between the near-surface atmospheric temperature extremes over Eastern Europe and East Asia. Although the teleconnections of heat extremes have received attention, the lead-lag details and the potential predictability on synoptic time scale have not been investigated clearly in previous studies (Deng et al. [42]; Kornhuber et al. [39]; Yang et al. [40]). About 3–4 days before the appearance of East Asian heatwaves, Eastern European heatwaves occur, accompanied by an intensified tropospheric anomalous anticyclone. A Rossby wave train, as a part of a CGT-like pattern, is triggered and propagates eastward, with alternative anomalies of high and low pressures over the Eurasian continent. Subsequently, another middle- and upper-tropospheric anomalous anticyclone in the downstream region causes sudden surface warming over East Asia as a result of both enhanced subsidence-related adiabatic heating and increased downward solar radiation due to reduced cloud cover. Thus, the eastward propagating wave train plays a vital role in linking the teleconnection of heat extremes over the Eurasian continent. Quantificationally, 43 % of East Asian heatwave events are preceded by Eastern European heatwave events in the 10-day time range before East Asian heatwave events. The investigation of heatwave teleconnection in the two remotes regions has strong potential to improve the prediction skill of East Asian heatwaves.

The standard deviations (σ) of East Asian and Eastern European daily *T*2m are 2.07 K and 1.57 K, respectively. It is noted that a pronounced surface warming anomaly over Eastern Europe ($\sim 1.45\,\mathrm{K} = 0.7\,\sigma$, $p < 0.01$) is observed before the East Asian heatwaves (Fig. 5a). By contrast, the East Asian surface warming anomaly is weaker ($\sim 0.55\,\mathrm{K} = 0.35\,\sigma$, $0.01 < p < 0.05$) after the

Eastern European heatwaves (Fig. 5c). The asymmetrical connection of heat extremes over the two distant regions deserves further investigations. Furthermore, a similar wave train is observed related to the springtime East Asian heatwaves (Zhang et al. [53]), emphasizing the significance of investigating the extreme event teleconnection in the transitional season. Moreover, East Asian heatwaves are also influenced by tropical forcings, such as the Pacific-Japan teleconnection pattern (Xu et al. [54]) and the Indian Ocean heat source (Gao et al. [55]), which deserves more awareness, especially under the large impacts of significant changes in the atmospheric convection over the western Pacific Ocean (Chen et al. [56]; Lin et al. [57]).

***Acknowledgements*:** The authors wish to thank Prof. WANG Zi-qian at Sun Yat-sen University for the useful discussion.

REFERENCES

[1] FISCHER E M, SCHÄR C. Consistent geographical patterns of changes in high-impact European heatwaves [J]. Nature Geoscience, 2010, 3: 398–403, https://doi.org/10.1038/ngeo866

[2] PERKINS S E, ALEXANDER L V, NAIRN J R. Increasing frequency, intensity and duration of observed global heatwaves and warm spells [J]. Geophysical Research Letters, 2012, 39(20): L20714, https://doi.org/10.1029/2012GL053361

[3] WESTERLING A L, HIDALGO H G, CAYAN D R, et al. Warming and earlier spring increase western US forest wildfire activity [J]. Science, 2006, 313(5789): 940–943, https://doi.org/10.1126/science.1128834

[4] THORNTON P K, VAN DE STEEG J, NOTENBAERT A, et al. The impacts of climate change on livestock and livestock systems in developing countries: A review of what we know and what we need to know [J]. Agricultural Systems, 2009, 101(3): 113–127, https://doi.org/10.1016/j.agsy.2009.05.002

[5] MENG Wei-guang, ZHANG Yan-xia, LI Jiang-nan, et al. Application of WRF/UCM in the simulation of a heat wave event and urban heat island around Guangzhou [J]. Journal of Tropical Meteorology, 2011, 17(3): 257–267.

[6] RÜBBELKE D, VÖGELE S. Impacts of climate change on European critical infrastructures: the case of the power sector [J]. Environmental Science & Policy, 2011, 14(1): 53–63, https://doi.org/10.1016/j.envsci.2010.10.007

[7] COUMOU D, RAHMSTORF S. A decade of weather extremes [J]. Nature Climate Change, 2012, 2(7): 491–496, https://doi.org/10.1038/nclimate1452

[8] LESK C, ROWHANI P, RAMANKUTTY N. Influence of extreme weather disasters on global crop production [J]. Nature, 2016, 529(7584): 84–87, https://doi.org/10.1038/nature16467

[9] FOUILLET A, REY G, LAURENT F, et al. Excess mortality related to the August 2003 heat wave in France [J]. International Archives of Occupational and Environmental Health, 2006, 80(1): 16–24, https://doi.org/10.1007/s00420-006-0089-4

[10] GARCÍA-HERRERA R, DÍAZ J, TRIGO R M, et al. A review of the European summer heat wave of 2003 [J]. Critical Reviews in Environmental Science and Technology, 2010, 40(4): 267–306, https://doi.org/10.1080/10643380802238137

[11] LAAIDI K, ZEGHNOUN A, DOUSSET B, et al. The impact of heat islands on mortality in Paris during the August 2003 heat wave [J]. Environmental Health Perspectives, 2012, 120(2): 254–259, https://doi.org/10.1289/ehp.1103532

[12] BARRIOPEDRO D, FISCHER E M, LUTERBACHER J, et al. The hot summer of 2010: redrawing the temperature record map of Europe [J]. Science, 2011, 332(6026): 220–224, https://doi.org/10.1126/science.1201224

[13] DOLE R, HOERLING M, PERLWITZ J, et al. Was there a basis for anticipating the 2010 Russian heat wave? [J] Geophysical Research Letters, 2011, 38(6): L06702, https://doi.org/10.1029/2010GL046582

[14] RUSSO S, SILLMANN J, FISCHER E M. Top ten European heatwaves since 1950 and their occurrence in the coming decades [J]. Environmental Research Letters, 2015, 10(12): 124003, https://doi.org/10.1088/1748-9326/10/12/124003

[15] DUCHEZ A, FRAJKA-WILLIAMS E, JOSEY S, et al. Drivers of exceptionally cold North Atlantic Ocean temperatures and their link to the 2015 European heat wave [J]. Environmental Research Letters, 2016, 11(7): 074004, https://doi.org/10.1088/1748-9326/11/7/074004

[16] WANG Z, LUO H, YANG S. Different mechanisms for the extremely hot central-eastern China in July–August 2022 from a Eurasian large-scale circulation perspective [J]. Environmental Research Letters, 2023, 18: 024023, https://doi.org/10.1088/1748-9326/acb3e5

[17] PERKINS S E, ALEXANDER L V. On the measurement of heat waves [J]. Journal of Climate, 2013, 26(13): 4500–4517, https://doi.org/10.1175/JCLI-D-12-00383.1

[18] HAO Z, CHEN Y, FENG S, et al. The 2022 Sichuan-Chongqing spatio-temporally compound extremes: a bitter taste of novel hazards [J]. Science Bulletin, 2013, 68: S2095–9273, https://doi.org/10.1016/j.scib.2023.05.034

[19] MAZDIYASNI O, AGHAKOUCHAK A. Substantial increase in concurrent droughts and heatwaves in the United States [J]. Proceedings of the National Academy of Sciences, 2015, 112(37): 11484–11489, https://doi.org/10.1073/pnas.1422945112

[20] PERKINS-KIRKPATRICK S E, LEWIS S C. Increasing trends in regional heatwaves [J]. Nature Communications, 2020, 11(1): 1–8, https://doi.org/10.1038/s41467-020-16970-7

[21] ROUSI E, KORNHUBER K, BEOBIDE-ARSUAGA G, et al. Accelerated western European heatwave trends linked to more-persistent double jets over Eurasia [J]. Nature Communications, 2022, 13(1): 1–11, https://doi.org/10.1038/s41467-022-31432-y

[22] MEEHL G A, TEBALDI C. More intense, more frequent, and longer lasting heat waves in the 21st century [J]. Science, 2004, 305(5686): 994–997, https://doi.org/10.1126/science.1098704

[23] COUMOU D, ROBINSON A. Historic and future increase in the global land area affected by monthly heat extremes [J]. Environmental Research Letters, 2013, 8(3): 034018, https://doi.org/10.1088/1748-9326/8/3/034018

[24] CHRISTIDIS N, JONES G S, STOTT P A. Dramatically increasing chance of extremely hot summers since the 2003 European heatwave [J]. Nature Climate Change, 2015, 5(1): 46–50, https://doi.org/10.1038/nclimate2468

[25] KING A D, HARRINGTON L J. The inequality of climate change from 1.5 to 2 °C of global warming [J]. Geophysical Research Letters, 2018, 45(10): 5030–5033, https://doi.org/10.1029/2018GL078430

[26] ZHANG Tuan-tuan, TAM Chi-yung, LAU Ngar-cheung, et al. Influences of boreal winter Arctic Oscillation on the peak-summer compound heat waves over the Yangtze-Huaihe River basin: the North Atlantic capacitor effect [J]. Climate Dynamics, 2022, 59: 2331–2343, https://doi.org/10.1007/s00382-022-06212-5

[27] ZSCHEISCHLER J, SENEVIRATNE S I. Dependence of drivers affects risks associated with compound events [J]. Science Advances, 2017, 3(6): e1700263, https://doi.org/10.1126/sciadv.1700263

[28] SARHADI A, AUSÍN M C, WIPER M P, et al. Multidimensional risk in a nonstationary climate: joint probability of increasingly severe warm and dry conditions [J]. Science Advances, 2018, 4(11): eaau3487, https://doi.org/10.1126/sciadv.aau3487

[29] BOERS N, BOOKHAGEN B, MARWAN N, et al. Complex networks identify spatial patterns of extreme rainfall events of the South American monsoon system [J]. Geophysical Research Letters, 2013, 40(16): 4386–4392, https://doi.org/10.1002/grl.50681

[30] BOERS N, BOOKHAGEN B, BARBOSA H M, et al. Prediction of extreme floods in the eastern Central Andes based on a complex networks approach [J]. Nature Communications, 2014, 5(1): 1–7, https://doi.org/10.1038/ncomms6199

[31] BOERS N, GOSWAMI B, RHEINWALT A, et al. Complex networks reveal global pattern of extreme-rainfall teleconnections [J]. Nature, 2019, 566(7744): 373–377, https://doi.org/10.1038/s41586-018-0872-x

[32] GUPTA S, SU Z, BOERS N, et al. Interconnection between the Indian and the East Asian summer monsoon: spatial synchronization patterns of extreme rainfall events [J]. International Journal of Climatology, 2022, 43(2): 1034–1049, https://doi.org/10.1002/joc.7861

[33] SU Z, MEYERHENKE H, KURTHS J. The climatic interdependence of extreme-rainfall events around the globe [J]. Chaos: An Interdisciplinary Journal of Nonlinear Science, 2022, 32(4): 043126, https://doi.org/10.1063/5.0077106

[34] LAU W K, KIM K M. The 2010 Pakistan flood and Russian heat wave: teleconnection of hydrometeorological extremes [J]. Journal of Hydrometeorology, 2012, 13(1): 392–403, https://doi.org/10.1175/JHM-D-11-016.1

[35] CAPUA G, SPARROW S, KORNHUBER K, et al. Drivers behind the summer 2010 wave train leading to Russian heatwave and Pakistan flooding [J]. npj Climate and Atmospheric Science, 2021, 4(1): 1–14, https://doi.org/10.1038/s41612-021-00211-9

[36] LI Kai-wen, WANG Ming, LIU Kai. The study on compound drought and heatwave events in China using complex networks [J]. Sustainability, 2021, 13(22): 12774, https://doi.org/10.3390/su132212774

[37] MUKHERJEE S, MISHRA A K. Increase in compound drought and heatwaves in a warming world [J]. Geophysical Research Letters, 2021, 48(1): e2020GL090617, https://doi.org/10.1029/2020GL090617

[38] KORNHUBER K, OSPREY S, COUMOU D, et al. Extreme weather events in early summer 2018 connected by a recurrent hemispheric wave-7 pattern [J]. Environmental Research Letters, 2019, 14(5): 054002, https://doi.org/10.1088/1748-9326/ab13bf

[39] KORNHUBER K, COUMOU D, VOGEL E, et al. Amplified Rossby waves enhance risk of concurrent heatwaves in major breadbasket regions [J]. Nature Climate Change, 2020, 10(1): 48–53, https://doi.org/10.1038/s41558-019-0637-z

[40] YANG Xiao-ye, ZENG Gang, ZHANG Shi-yue, et al. Relationship between two types of heat waves in northern East Asia and temperature anomalies in Eastern Europe [J]. Environmental Research Letters, 2021, 16(2): 024048, https://doi.org/10.1088/1748-9326/abdc8a

[41] ZHOU Ye-fan, WU Zhi-wei. Possible impacts of mega - El Niño/Southern Oscillation and Atlantic Multidecadal Oscillation on Eurasian heatwave frequency variability [J]. Quarterly Journal of the Royal Meteorological Society, 2016, 142(697): 1647–1661, https://doi.org/10.1002/qj.2759

[42] DENG Kai-qiang, YANG Song, TING Ming-fang, et al. An intensified mode of variability modulating the summer heat waves in eastern Europe and northern China [J]. Geophysical Research Letters, 2018, 45(20): 11–361, https://doi.org/10.1029/2018GL079836

[43] HERSBACH H, BELL B, BERRISFORD P, et al. ERA5 hourly data on pressure levels from 1959 to present [Z]. Copernicus Climate Change Service (C3S) Climate Data Store (CDS), 2018, https://doi.org/10.24381/cds.bd0915c6

[44] YASUI S, WATANABE M. Forcing processes of the summertime circumglobal teleconnection pattern in a dry AGCM [J]. Journal of Climate, 2010, 23(8): 2093–2114, https://doi.org/10.1175/2009JCLI3323.1

[45] CEN Si-xian, CHEN Wen, CHEN Shang-feng, et al. Potential impact of atmospheric heating over eastern Europe on the zonal shift in the South Asian high: the role of the Silk Road teleconnection [J]. Scientific Reports, 2020, 10(1): 1–10, https://doi.org/10.1038/s41598-020-63364-2

[46] TAKAYA K, NAKAMURA H. A formulation of a phase-independent wave-activity flux for stationary and migratory quasigeostrophic eddies on a zonally varying basic flow [J]. Journal of the Atmospheric Sciences, 2001, 58(6): 608–627, https://doi.org/10.1175/1520-0469(2001)058<0608:AFOAPI>2.0.CO;2

[47] DENG K, YANG S, TING M, et al. Dominant modes of China summer heat waves driven by global sea surface temperature and atmospheric internal variability [J]. Journal of Climate, 2019, 32(12): 3761–3775, https://doi.org/10.1175/JCLI-D-18-0256.1

[48] DENG Kai-qiang, YANG Song, TING Ming-fang, et al. More frequent summer heat waves in southwestern China linked to the recent declining of Arctic sea ice [J]. Environmental Research Letters, 2020, 15(7): 074011, https://doi.org/10.1088/1748-9326/ab8335

[49] ZHOU Fu-li, ZHANG Ren-he, HAN Jin-ping. Influences of the East Asian summer rainfall on circumglobal teleconnection [J]. Journal of Climate, 2020, 33(12):

5213–5221, https://doi.org/10.1175/JCLI-D-19-0325.1

[50] DING Qing-hua, WANG Bin. Circumglobal teleconnection in the Northern Hemisphere summer [J]. Journal of Climate, 2005, 18(17): 3483–3505, https://doi.org/10.1175/JCLI3473.1

[51] LU R Y, OH J H, KIM B J. A teleconnection pattern in upper-level meridional wind over the North African and Eurasian continent in summer [J]. Tellus A: Dynamic Meteorology and Oceanography, 2002, 54(1): 44–55, https://doi.org/10.3402/tellusa.v54i1.12122

[52] WANG Zi-qian, YANG Song, LUO Hao-lin, et al. Drying tendency over the southern slope of the Tibetan Plateau in recent decades: role of a CGT-like atmospheric change [J]. Climate Dynamics, 2022, 59: 2801–2813, https://doi.org/10.1007/s00382-022-06262-9

[53] ZHANG Tuan-tuan, JIANG Xing-wen, CHEN Jun-wen, et al. Interannual variability of springtime extreme heat events over the southeastern edge of the Tibetan Plateau: role of a spring-type circumglobal teleconnection pattern [J]. Journal of Climate, 2021, 34(24): 9915–9930, https://doi.org/10.1175/JCLI-D-21-0049.1

[54] XU K, LU R, KIM B, et al. Large-scale circulation anomalies associated with extreme heat in South Korea and southern–central Japan [J]. Journal of Climate, 2019, 32 (10): 2747–2759, https://doi.org/10.1175/JCLI-D-18-0485.1

[55] GAO Qing-Jiu, LI Yan, HAN Tong-xin. Intra-seasonal features of an extreme high temperature event in 2011 in Eastern China and its atmospheric circulation [J]. Journal of Tropical Meteorology, 2021, 27(4): 437–446, https://doi.org/10.46267/j.1006-8775.2021.038

[56] CHEN Jia-xin, HU Xiao-ming, YANG Song, et al. Influence of convective heating over the Maritime Continent on the west Antarctic climate [J]. Geophysical Research Letters, 2022, 49(9): e2021GL097322, https://doi.org/10.1029/2021GL097322

[57] LIN Shu-heng, YANG Song, HE Shan, et al. Attribution of the seasonality of atmospheric heating changes over the western tropical Pacific with a focus on the spring season [J]. Climate Dynamics, 2022, 58(9): 2575–2592, https://doi.org/10.1007/s00382-021-06020-3

Citation: CAI Fen-ying, LIU Cai-hong, YANG Song, et al. Linkage Between European and East Asian Heatwaves on Synoptic Scales [J]. Journal of Tropical Meteorology, 2024, 30(2): 97–105, https://doi.org/10.3724/j.1006-8775.2024.010